7th International Shock Tube Symposium, Institute for Aerospace Studies, University of Toronto, June 23-25, 1969.

[4] Tiemann, W., "Gas Dynamic Phenomena During the Dark Phase of Wire Explosions and Their Importance for Reignition," TTF-12,430, Aug. 1969, NASA.

[5] Cobine, J. D., *Gaseous Conductors, Theory and Engineering*, Dover, New York, 1941, p. 164.

[6] Mullaney, G. J. and Ahlstrom, H. G., "Energy Transfer Mechanism in Shock-Tube Arc-Heated Drivers," *AIAA Journal*, Vol. 7, No. 7, July 1969, pp. 1353-6.

[7] Goldstein, R. and Mastrup, F. N., "Radiation Measurements from a Pulsed High-Pressure Nitrogen Arc," Final Rept. ARL-68-0152, Aug. 1968, TRW, Inc., Redondo Beach, Calif.

[8] Glass, I. I., "Aerodynamics of Blasts," UTIAS Review No. 17, University of Toronto, Toronto, Canada, Sept. 1960.

[9] Webb, F. H., Jr., et al., "The Electrical and Optical Properties of Rapidly Exploded Wires," *Exploding Wires*, Vol. 2, Plenum Press, New York, 1962, pp. 37-75.

An Exact Differential Method to Determine Liapunov Stability

M. A. RAHMAN*
NASA Manned Spacecraft Center, Houston, Texas

IN this Note a simple method is presented to find the time derivative of a Liapunov function[1,2,3] in order to test the asymptotic stability of an autonomous system. The concepts[1,2,3] of Liapunov's function are not presented here. However, it may be mentioned that if the Liapunov function in the study of motion of a system is positive definite and its total rate of change with respect to time is negative definite or negative semidefinite, then the motion of the system is considered to be asymptotically stable.

The Liapunov function $V(x)$ is a scalar, and it is not unique. The line integral[4] between two points is independent of the path of integration, and it is assumed that the curl grad V is equal to zero.

In the analysis of the motion of a system, we obtain a system of equations of motion. Utilizing the state variable analysis,[2] we may reduce the equations of motion into a set of state variable equations. Without solving these equations, we may determine the asymptotic stability of the motion by employing the Liapunov stability criteria in the following formulations:

$$\text{Let } V = \int_{p_1}^{p_2} d[\Sigma x_i^2 x_j^2]; \quad i,j = 1,2, \ldots n \tag{1}$$

For brevity, we consider 3-dimensional case in Eq. (1) and obtain

$$V = \int_{p_1}^{p_2} [(4x_1^3 + 4x_1x_2^2 + 4x_1x_3^2)dx_1 + (4x_2^3 + 4x_2x_3^2 + 4x_2x_1^2)dx_2 + (4x_3^3 + 4x_3x_1^2 + 4x_3x_2^2)dx_3] \tag{2}$$

Recalling that the integral of a gradient is independent of the path of integration, we write

$$V = \int_{p_1}^{p_2} \left[\frac{\partial V}{\partial x_1} dx_1 + \frac{\partial V}{\partial x_2} dx_2 + \ldots + \frac{\partial V}{\partial x_n} dx_n\right] \tag{3}$$

For 3-dimensional case

$$V = \int_{p_1}^{p_2} \left[\frac{\partial V}{\partial x_1} dx_1 + \frac{\partial V}{\partial x_2} dx_2 + \frac{\partial V}{\partial x_3} dx_3\right] \tag{4}$$

Using the exactness criteria, we get from Eqs. (2) and (4),

$$\begin{aligned} \partial V/\partial x_1 &= 4x_1^3 + 4x_1x_2^2 + 4x_1x_3^2 \\ \partial V/\partial x_2 &= 4x_2^3 + 4x_2x_3^2 + 4x_2x_1^2 \\ \partial V/\partial x_3 &= 4x_3^3 + 4x_3x_1^2 + 4x_3x_2^2 \end{aligned} \tag{5}$$

And the time derivative $\dot{V}(x)$ is

$$dV/dt = \Sigma(\partial V/\partial x_i)\dot{x}_i; \quad i = 1,2, \ldots n \tag{6}$$

The procedures are explained by an example.

Let us consider the system

$$\dot{x}_1 = -x_2 - x_1^3; \quad \dot{x}_2 = x_1 - x_2 \tag{7}$$

using Eqs. (5) and (6), we get for 2-dimensional case

$$\begin{aligned} dV/dt &= (4x_1^3 + 4x_1x_2^2)(-x_2 - x_1^3) + (4x_2^3 + 4x_2x_1^2)(x_1 - x_2) \\ &= -(4x_1^6 + 4x_2^4 + 4x_1^4x_2^2 + 4x_2^2x_1^2) \end{aligned}$$

which is negative definite. Therefore, the system [Eq. (7)] is asymptotically stable.

As far as line integral and the assumptions are concerned, this technique has similarity only with the existing variable-gradient method.[2] An iterative procedure is required to determine the coefficients of the gradient matrix in the variable-gradient method. Although the partial derivative of an arbitrary positive definite function $V(x)$ with respect to the state variables may lead to some results, the exactness approach in the field of curl grad $V = 0$ may establish a mathematical criteria for a methodology.

References

[1] Krasovskii, N. N., "Stability of Motion," translated by J. L. Brenner, Stanford University Press, Stanford, Calif., 1963, Chap. 1, pp. 11-43.

[2] Timothy, L. K. and Bona, B. E., "State Space Analysis," McGraw-Hill, New York, 1968, Chap. 7, pp. 239-279; also Chap. 4, pp. 103-160.

[3] Chan, C.-F. and Haas, J. I., "Elements of Control System Analysis," Prentice Hall, Englewood Cliffs, N.J., 1968, Chap. 8, pp. 386-446.

[4] Kaplan, W., *Advanced Calculus*, Addison-Wesley, Reading, Mass., 1959, Chap. 5, pp. 225-301.

Received June 4, 1970; revision received August 31, 1970. The author gratefully acknowledges the computer verification of the results done by Jon C. Axford of Flight Procedures Branch, NASA Manned Spacecraft Center, Houston, Texas.

* Aerospace Engineer, Fluid and Flight Mechanics. Member AIAA.

Vibration Analysis by Differential Holographic Interferometry

R. APRAHAMIAN* AND D. A. EVENSEN†
TRW Systems Group, Redondo Beach, Calif.

A NEW double-pulse method of holographic interferometry is proposed. This technique intends holography to permit measurements on large, noisy subjects vibrating to

Received September 17, 1970.

* Member of the Advanced Technology Department, Applied Mechanics Laboratory. Member AIAA.

† Member of the Advanced Technology Department, Applied Mechanics Laboratory.

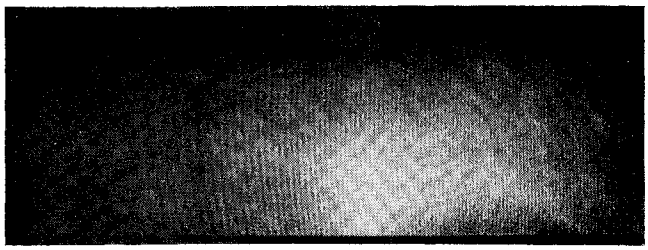

Fig. 1 Differential interferogram of a vibrating plate.

large amplitudes. The method is demonstrated experimentally using a large aluminum plate.

Time average holography[1] and stored-beam interferometry[2] are limited in application to small amplitude vibrations. If large amplitudes are used with these holographic techniques, the interference fringes crowd closely together in regions of high slopes and cannot be readily distinguished from one another. For example, a surface slope of 6×10^{-4} radians corresponds to a fringe spacing of 0.01 in. when light of 6328 Å is used. Larger surface slopes result in even closer fringe spacing. This limitation on allowable vibration amplitudes is a fundamental drawback to applying holography with large-scale, flexible structures.

Another limitation of the holographic techniques used to date for vibration analysis is the fact that the entire system must be isolated from background vibrations and noise. This isolation requirement presents a problem when large-scale structures are involved.

Finally, most continuous-wave lasers currently available do not have sufficient light output for holographic vibration analysis of large-scale structures.

To overcome these limitations of present techniques for holographic vibration analysis, the use of pulsed laser holography appears very promising. Consider what happens if a structure is vibrating, sinusoidally in a normal mode, and a double exposure hologram is made by pulsing the laser once at time t_1 and again at time t_2. From the first pulse, we have the displacement

$$w_1(\mathbf{x},t) = A\Phi(\mathbf{x}) \sin\omega t_1$$

where A is the vibration amplitude, $\Phi(\mathbf{x})$, represents the mode shape, ω is the vibration frequency, and t_1 is the time of the first exposure. The second pulse at time t_2 gives the displacement

$$w_2(\mathbf{x},t) = A\Phi(\mathbf{x}) \sin\omega t_2$$

The interference pattern which forms is a measure of the difference in displacements at time t_1 and t_2. Thus, the interference pattern is proportional to

$$w_1 - w_2 = A\Phi(\mathbf{x})[\sin\omega t_1 - \sin\omega t_2]$$

$$= K\Phi(\mathbf{x})$$

where K is a constant representing the product $A[\sin\omega t_1 - \sin\omega t]$. By adjusting the times t_1 and t_2 to be close together, only a few interference fringes will be formed, regardless of the amplitude of vibration. From this fringe pattern, the mode shape $\Phi(\mathbf{x})$ can be found. This technique of double-pulsing thus eliminates the restriction of small amplitude vibrations.

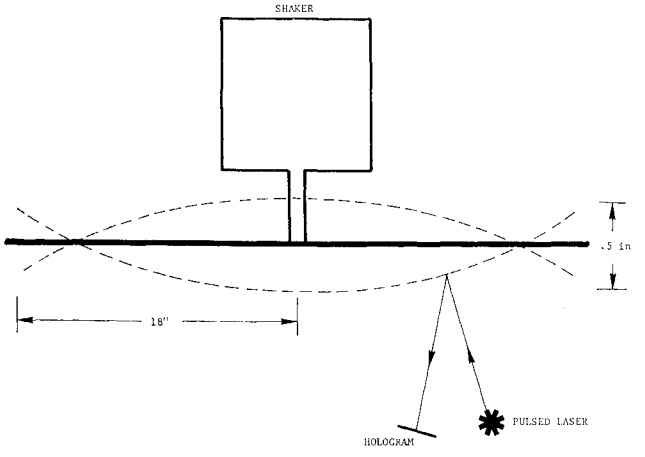

Fig. 2 Pulsed laser and vibrating plate schematic arrangement.

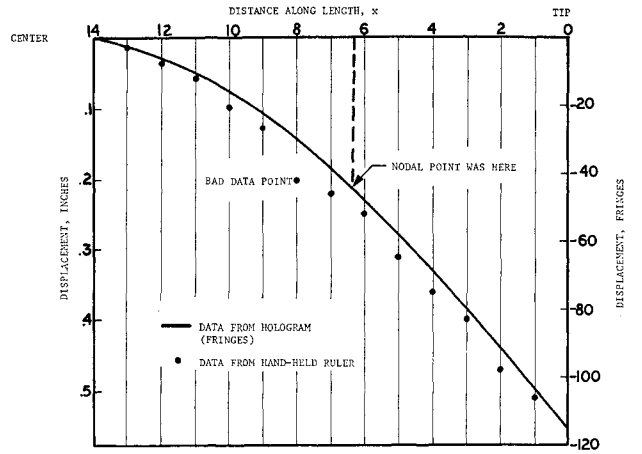

Fig. 3 Measured vibration shape for large aluminum plate.

In addition, since the duration of each laser pulse is on the order of 10^{-8} sec, the recording of the hologram is not influenced by seismic disturbances and other background noise. Finally, the high-intensity pulse available from a conventional ruby laser makes holographic interferometry possible for large-scale structures (e.g., a 10 × 10-ft area).

An example of a hologram of a vibrating object made by this double-pulse method is shown in Fig. 1. The vibrating specimen was a piece of aluminum sheet, 6 in. wide and 36 in. long, supported at the center on the armature of a shaker. (See schematic, Fig. 2.) Only the right half of the specimen is shown in Fig. 1. The laser was pulsed at times t_1 and t_2 with a 50 μsec delay between pulses. Notice that the number of fringes formed was not unduly large, although the plate was vibrating with a peak-to-peak displacement of $\frac{1}{2}$ in. at the tip.

The vibration shape indicated by the hologram is compared with data obtained by direct measurement and shown in Fig. 3. The circled data points in Fig. 3 were obtained using a hand-held ruler and measuring the peak-to-peak displacement at locations along the length at one-inch intervals. The solid line was obtained by counting the fringes in Fig. 1, choosing as zero a point 14 in. from the tip of the beam. Each fringe in Fig. 1 indicates a normal displacement of $\lambda/2$ from the neighboring fringes. The data have been scaled such that 115 fringes is equivalent to 0.55 in., making the first and last points of the two data sets coincide. In general, the agreement between the two measurement schemes is quite good, with the differences being less than $\frac{1}{20}$ of an inch. This is within the tolerance achievable with the hand-held ruler.

Figures 1–3 demonstrate that pulsed laser holograms can be made and analyzed in the manner just described. These results are particularly significant for future applications of holography to vibrations, since they demonstrate that experimenters are no longer limited to small amplitude motions. From the experiment described here, the way to future holographic vibration analysis of large-scale structures seems fairly clear.

References

[1] Powell, R. L. and Stetson, K. A., "Interferometric Vibration Analysis by Wavefront Reconstruction," *Journal of the Optical Society of America*, Vol. 55, No. 12, Dec. 1965, pp. 1593–1598.

[2] Stetson, K. A. and Powell, R. L., "Interferometric Hologram Evaluation and Real-Time Vibration Analysis of Diffuse Objects," *Journal of the Optical Society of America*, Vol. 55, No. 12, 1965, 1694–1695.

Turbulent Boundary-Layer Flow over a Rotating Flat-Plate Blade

W. J. McCroskey*
U. S. Army Aeronautical Research Laboratory, Moffett Field, Calif.
AND
J. F. Nash† AND J. G. Hicks‡
Lockheed-Georgia Research Laboratory, Marietta, Ga.

TURBULENT boundary layers on rotating blades have not been studied as extensively as laminar flows, although turbulence is common in practical applications, such as propellers and helicopter rotors. This Note is concerned with a set of calculated results for the incompressible turbulent flow over a steadily rotating flat-plate blade, for flow conditions that in the laminar case were found by Dwyer and McCroskey[1] to produce strong three-dimensional effects, such as centrifugal pumping and an increase in the shear stress at the wall. One of the main points of interest here is the extent to which certain qualitative features of laminar and turbulent flows are alike, whereas the quantitative details are significantly different.

The calculations described in this Note were performed using the recent method of Nash,[2] modified by the inclusion of the Coriolis and centrifugal terms in the two mean-flow momentum equations, following Ref. 1. The assumptions concerning the shear stress were left unchanged. These assumptions are that the shear stress can be determined from the empirically modified turbulent kinetic-energy equation, formulated by Bradshaw et al.,[3] for two-dimensional flow, together with the additional assumption that the local shear-stress vector acts in the direction of the local mean rate of strain. Otherwise, two-dimensional turbulent physics is assumed to apply.

Following the notation of Ref. 1 (shown here in Fig. 1), the calculations were started at initial chordwise x stations such that a laminar boundary layer growing from the leading edge would have attained a momentum thickness Reynolds number of 380. At this point "transition" to an initial turbulent velocity profile, with $Re_\theta = 380$ and $Re_\delta = 3000$, was assumed to occur. This starting procedure was found to be effective in reducing the sensitivity of the results to variations of local unit Reynolds number, $\Omega z/\nu$. The range of Reynolds numbers considered was from 3.5×10^6 to 5×10^8, based on the maximum distance from the leading edge; this range covers both marine and aeronautical applications.

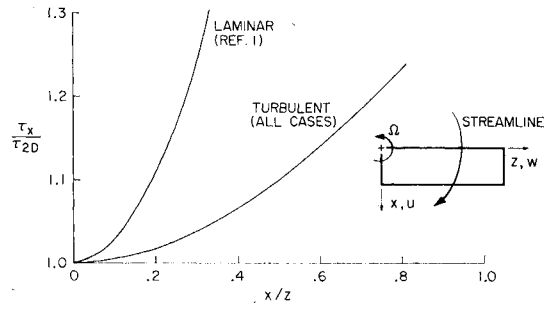

Fig. 1 Chordwise wall shear-stress distribution on a rotating flat-plate blade.

One of the most important results from the previous laminar investigation[1] was that the three-dimensional departures from two-dimensional flow, or "strip theory" results, correlated uniquely with the parameter x/z. Furthermore, the chordwise component of the surface shear stress was found to provide a good basis for indicating the over-all significance of crossflow and rotational effects. Therefore, the ratio of the component of the wall shear stress in the x direction to the local "strip theory" value is shown in Fig. 1 as a function of x/z. All of the turbulent results were found to collapse essentially to the single curve shown. Just as in the laminar case, the wall shear increases with increasing x/z, although the rate of increase is considerably less in the present case.

There is a subtlety associated with Fig. 1 that deserves further consideration. Unlike the laminar results, the increase in the turbulent shear stress coincides almost exactly with the results of a simple-minded locally two-dimensional flow based on the total external velocity at each point; that is, a nonrotating flat-plate boundary layer which has a local external velocity equal to $(U_e^2 + W_e^2)^{1/2}$ and no boundary-layer crossflow relative to the local potential-flow streamline. This is consistent with the small crossflow in the actual three-dimensional boundary layer. Figure 2 shows the variation of the wall crossflow angle, i.e., the angle between the surface streamlines and the inviscid-flow streamlines. Even at the lowest Reynolds numbers,§ this angle is less than 3° for values of x/z up to 0.8. For the hovering flat plate, of course, the potential-flow streamlines are circular arcs.

A further illustration of the nature of the crossflow is provided by Fig. 3, which shows the velocity profiles in the radial direction rather than spanwise. The fluid close to the wall, whether laminar or turbulent, is centrifuged radially outward. The quantitative differences can be explained by recalling that turbulent flow near a wall has a much smaller tangential momentum defect and larger shear stress gradients than laminar flow; therefore, it is not surprising that the centrifugal pumping effect should be an order of magnitude smaller for the turbulent case. It is interesting to note that in either case the radial velocity increases approximately linearly

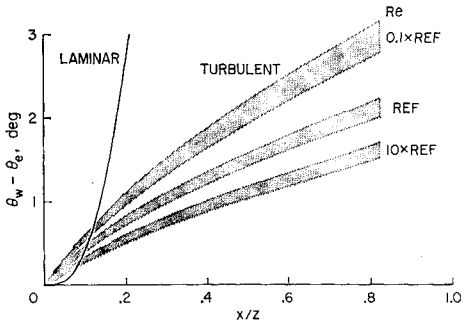

Fig. 2 Surface streamline direction relative to the local inviscid flow.

Received September 28, 1970.
* Research Scientist. Member AIAA.
† Scientist. Member AIAA.
‡ Associate Scientist.

§ Unlike the shear stress ratio in Fig. 1, the flow direction exhibits a slight systematic dependence upon Reynolds number. The reference Reynolds numbers, $\Omega xz/\nu$, were based upon $\Omega = 23$ rad/sec, 17 ft $\leq z \leq$ 25 ft, $0 < x \leq 13.7$ ft, and $\nu = 1.56 \times 10^{-4}$ ft^2/sec.